Printing Strain Gauges on Intuitive Surgical da Vinci Robot End Effectors

Rut Peña*[1,2], Michael J. Smith*[1,2], Nicolas P. Ontiveros[1], Frank L. Hammond III[3], and Robert J. Wood[1,2]

***Abstract*— Force feedback during robotic surgery is critical in order to minimize potential injury to the patient and decrease recovery time from surgical procedures. Here we describe the use of a novel strain gauge printing method to apply low profile, low cost sensors directly to the surface of da Vinci surgical robot end effectors (Intuitive Surgical, Inc.) to sense deflection and provide force feedback. This additive, vapor-deposition-based sensor fabrication method is used to deposit strain gauges directly onto the surfaces of the end effectors with minimal disruption to the device and without the need for adhesives or machining operations. Initial experiments characterize sensor performance and indicate the applicability of the proposed approach for force feedback during minimally invasive procedures.**

I. Introduction

The use of robotics in MIS (Minimally Invasive Surgery) has improved the quality of care for a number of procedures. Benefits include a reduction in recovery time, postoperative pain, and reduced cost of treatment [1], [2], [3], [4], [5]. However, there are a number of unresolved challenges that have the potential to further benefit these outcomes. Since the operator (surgeon) is mechanically decoupled from the surgical workspace, there is a disconnect in the haptic feeling and perception of the overall procedure. Integrated haptic feedback may help to improve some clinical procedures by allowing the surgeon to feel the forces that the instrument is applying to the local environment and therefore prevent damage to tissue or instruments due to excessive loading. Excessive forces at the instrument point of contact can lead to procedural complications and decreased quality of treatment [6]. A key aspect to allow force-feedback will be to have a good estimation of the forces applied at the end effector throughout the surgery. Tissue tensioning during surgical procedures can require forces up to 2 N at the point of contact [7], and robotic end effectors may deflect up to 15 mm during surgery leading to errors in instrument positioning if these are not compensated for, which can ultimately lead to decreased efficacy of the task [8]. Even though there are a number of solutions to measure or estimate forces at the end-effector, their widespread adoption is limited since existing sensors add significant mass and volume, require complicated custom manufacturing techniques or adhesives, lack robustness to sterilization, are not compatible with existing surgical end-effectors, or are cost-prohibitive [9]. Available sensors to measure tool-tissue interaction forces include customized force sensor to measure forces applied by a forceps during microsurgery [10], soft liquid-embedded tactile sensors [11], and silicon-based strain gauges [12], [13]. Capacitive sensors are another option to measure contact properties, in particular force and pressure [14]. In addition, piezoelectric-based sensors using PVDF (polyvinylidene fluoride) have been integrated into minimally invasive surgical tools for haptic sensing [15]. Optical sensors such as embedded Fiber Bragg Gratings (FBG) have also demonstrated advantages due to their physical robustness, sensitivity, and immunity to electromagnetic interference [16], [17]. These techniques have created sensors with sufficient capabilities to measure forces during MIS. However, in addition to their cost, there are a number of challenges when implementing these tools in practice, such as the size of the sensor to meet the dimensions of the tools, the required surface conditioning of the tool to ensure proper adhesion, and robustness of the sensor to survive the sterilization process before and after surgery.

As an alternative to physical sensors integrated on the end effector, the drive motor current can be combined with dynamic models to estimate the force or strain of a particular degree of freedom of the robot [18]. However, these methods may lead to inaccurate estimation of strain and external forces due to factors such as frictional losses and nonlinearities in the drive-train.

In this paper, we present a method to print lightweight, low-volume sensors directly onto the surface of surgical instruments without the need for complicated machining processes or adhesives. We achieve this by using physical and chemical vapor deposition technology in a multi-layer strain gauge. This technique, derived from the work in [19], results in low-cost sensing that can be applied to flat surfaces as well as singly-curved surfaces allowing for the direct integration of sensors on robotic end effectors for force detection. We show that this method can be successfully applied to a variety of substrates and surface configurations. As a proof of concept, we describe the process to print strain sensors onto glass-reinforced composite shafts of the Large Needle Driver and the Fenestrated Grasper for the Intuitive Surgical da Vinci robot in a variety of configurations and gauge materials. Both end effectors have similar specifications, namely similar overall dimension and materials; the primary difference is the tool at the tip of the end effector. Section II includes an overview of the general gauge manufacturing process. Section III examines the application of this process to the da Vinci instruments and describes prototype fabrica-

* Authors contributed equally to this work.

[1] John A. Paulson School of Engineering and Applied Sciences, Harvard University, Cambridge, MA 02138, USA.

[2] The Wyss Institute for Biologically Inspired Engineering, Harvard University, Boston, MA 02115, USA.

[3] George W. Woodruff School of Mechanical Engineering, Georgia Institute of Technology, Atlanta, GA 30332, USA.

Please send correspondence to rut.pena@wyss.harvard.edu.

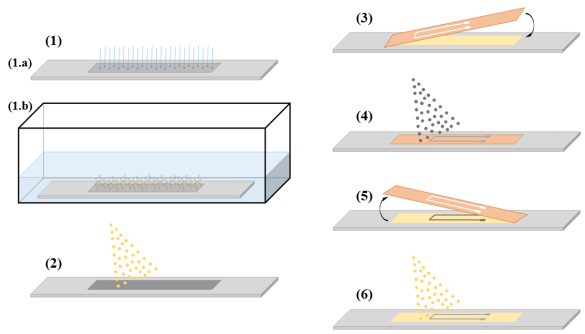

Fig. 1. Overview of the manufacturing steps: (1) Surface conditioning: (1.a) Sand blasting is used to roughen the surface followed by (1.b) silane etchant bath to promote adhesion between substrate and insulator. (2) Insulation: A thin layer of Parylene C is used to insulate the substrate from the metal gauge. (3) Masking: Kapton tape is cut accurately in the DPSS laser and place on the tool for selective sputtering. (4) Metallization: Sputter coating. (5) Mask removal. (6) Encapsulation: The gauge is coated with Parylene C to encapsulate and protect it.

tion. Section IV discusses bench-level testing and presents characterization results. Section V discusses conclusions and future research on this topic.

II. General Gauge Design and Manufacturing

Gauges are designed using the bulk material properties of the gauge metals and deposited onto the substrate surface using physical and chemical vapor deposition techniques. The process steps include (A) gauge design, (B) surface conditioning (if needed), (C) preliminary dielectric deposition using chemical vapor deposition (CVD), (D) masking using laser-micromachined contact masks, (E) metallization using physical vapor deposition (PVD), (F) CVD encapsulation, (G) electronics and signal processing and (H) EMI shielding. An overview of the manufacturing steps is shown in Fig. 1.

III. Application-Specific Manufacturing

A. Gauge Design and Material Considerations

The material used is Constantan, an alloy of 55% Copper and 45% Nickel. Its main feature is its resistivity, $5 \times 10^{-7}\Omega\cdot$m, which is constant over a wide range of temperatures. Constantan tends to exhibit a continuous drift at temperatures above 65°C [20], but common body and ambient temperatures are significantly lower than this temperature. It has also an adequately high strain sensitivity, good fatigue life and relatively high elongation capability. These properties needed for strain gauge applications make Constantan a suitable alloy for the printed sensors. In addition to Constantan, Karma has also been used, it is an alloy of Nickel, Chromium, Aluminum and Iron. Karma is characterized by good fatigue life and excellent stability, and it is appropriate for accurate strain measurements over long periods of time at room temperature, or shorter periods at high temperatures [21].

Serpentine gauges are designed for ease of manufacture and testing with a trace width of 400 μm and a thickness

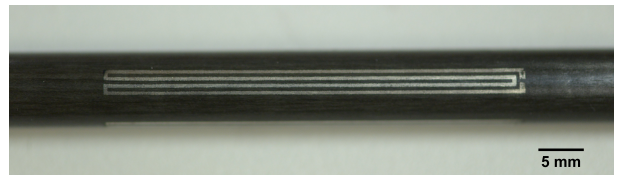

Fig. 2. Serpentine gauge pattern on the composite shaft of an Intuitive Surgical end effector.

of 0.816 μm (Fig. 2). The single serpentine design includes three turns with a total length of 0.180 m resulting in a predicted resistance of 1.552×10^3 Ω.

In the regime of small (e.g.,<1%) strain, ϵ is defined as

$$\epsilon = \frac{\Delta l}{l} \tag{1}$$

where Δl is the elongated length of the gauge and l is the unstrained length of the gauge. The gauge resistance change as a function of strain (i.e., the gauge factor, GF) is defined as

$$GF = \frac{\frac{\Delta R}{R}}{\epsilon} \tag{2}$$

where ΔR is the change in Constantan resistance due to strain induced by elongation and R is the unstrained resistance of the gauge. Because the gauge thickness ($<$ 1 μm) is negligible relative to the diameter of the target devices (8.3 mm), we assume the surface strain experienced by the gauge is identical to the strain experienced by the surface of the surgical device. This is given by

$$\epsilon = \frac{MZ}{EI} \tag{3}$$

where M is the bending moment experienced at the location of the gauge, Z is the distance from the neutral axis to the outer surface of the device shaft, E is the modulus of elasticity for the material (empirically determined), and I is the second moment of inertia for the geometry (annulus). The material modulus is derived from force and deflection values using a cantilever beam configuration on a materials testing machine (Instron model 5544) and calculated using beam theory:

$$E = \frac{FL^3}{D3I} \tag{4}$$

where F is the force perpendicular to the neutral axis at the distal end of the shaft and D is the distance of the distal end deflection (assuming these deflections correspond to the linear elastic range of the base material), and L is the length from the shaft distal end to the center of the deposited gauge. Expanding equation (3) results in

$$\epsilon = \frac{FLZ}{\frac{FL^3}{D3I}\frac{\pi}{2}(R_o^4 - R_i^4)} \tag{5}$$

where R_o is the distance from the neutral axis to the outer surface of the shaft and R_i is the distance from the neutral axis to the inner surface of the shaft. In the case of a Constantan gauge located 0.2 m from the distal end of the Large Needle Driver, gauge strain at a deflection of 30 mm

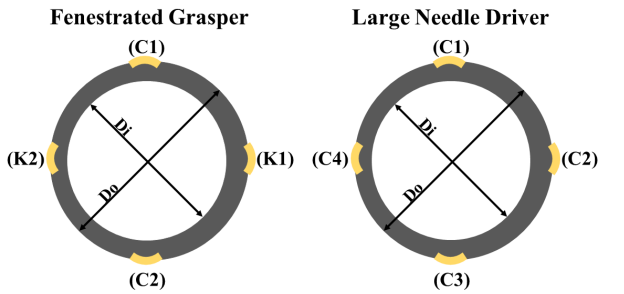

Fig. 3. Schematic cross sections of the shafts and strain gauge locations.

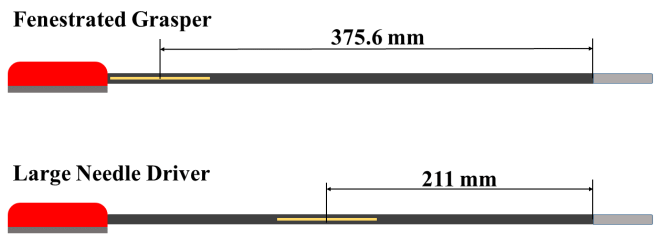

Fig. 4. Schematic representation of the strain gauge locations on the end effectors.

is predicted to be 0.38%. The predicted resistance change is 5.72 Ω, resulting in a predicted $GF = 0.969$.

For testing, Constantan (C) and Karma (K) gauges are placed 180° apart at 90° intervals around the circumference of the shaft for use in both single-sided and differential mode operation (Fig. 3). Two sensors, printed opposing each other, allow having two planes of strain detection. As one of the sensors experiences extension, the material on the opposite side is under compression. This configuration helps characterize the printed sensors as well as serves as a prognostic tool for sensor health since the absolute value of the change (resistance or voltage) should be the same when the force is applied.

In addition to the location of the sensors around the cross section, gauge pairs are placed at the mid-point of the Large Needle Driver for increased force range and at the proximal end of the shaft on the Large Fenestrated Grasper for increased sensitivity, as shown in Fig. 4. As a result of the non-uniformity of the strain along the shaft, these two locations allow for testing the sensors under different force configurations.

B. Surface Conditioning

On substrates such as metals and composites it is sometimes desirable to use surface preparations such as sand blasting or surface sanding to maximize adhesion of dielectric or metallization layers. Maximum bond strength to a metal surface is obtained using a combination of sand blasting beginning with an aggressive 250 μm aluminum oxide media followed by treatment with 100 μm aluminum oxide. Final surface preparation includes surface cleaning with isopropyl alcohol then application of a 1% mixture of Silane A-174, isopropyl alcohol, and deionized water for 30 minutes to etch surface oxides and impurities. In preparation for processing, the instruments are disassembled such that the composite shaft can be processed by itself. The shaft is then cut to fit in the smaller vapor and particle deposition chambers. This step would be eliminated with the use of larger processing equipment.

C. Dielectric Deposition

On metallic substrates it is desirable to apply a 50 μm base dielectric layer of Parylene C, a moisture resistant, low permittivity biocompatible polymer, before application of the gauge metallization. The adhesion of the dielectric layer to the substrate and deposited metallization is critical for proper adhesion, accurate transmission of the surface strain to the sensing element, and electrical isolation of the deposited signal-carrying traces. Dielectric deposition is carried out using the PDS 2010 Parylene deposition system (Specialty Coating Systems, Inc.). For the composite shaft of the da Vinci robotic end effector initial dielectric deposition is not needed.

D. Masking

Contact mask writing is carried out using a custom built 1.5 W DPSS (Diode Pumped Solid State) laser system. In this process, the mask is fabricated from 25 μm thick polymide (Kapton) tape (DuPont). The sample is placed into the DPSS system and cut at full power with the 10 μm wide beam moving at 20 cm/sec and retracing the cut geometry 25 times in order to produce smooth cuts with a minimum of recast material on the mask surface. Completed masks are positioned onto the surface of the prepared substrate, which is then placed into the PVD system for metal deposition.

E. Metallization

Deposition of the gauge and electrical trace metals are completed using a Denton Desktop Pro PVD system (Denton Vacuum LLC, Moorestown, NJ, USA). Deposition rates vary with material, copper was deposited at 109 nm/min, and constantan at 51 nm/min. Depositions are built up layer by layer with cooling cycles allowed between applications. The total sputtering time is 20 minutes and the final thickness is approximately 1 μm. Typically, the deposition chamber is operated with a duty cycle of one minute on, one minute off so that the machine, the substrate, and the masks are not subject to overheating.

Each end effector has four gauges, the initial resistance of the printed gauges ranges from 1500 to 2000 Ω (±100 Ω). Although the manufacturing process is similar, the difference in the initial resistance is likely due to manual steps during the manufacturing process that could introduce some differences in the electrical properties.

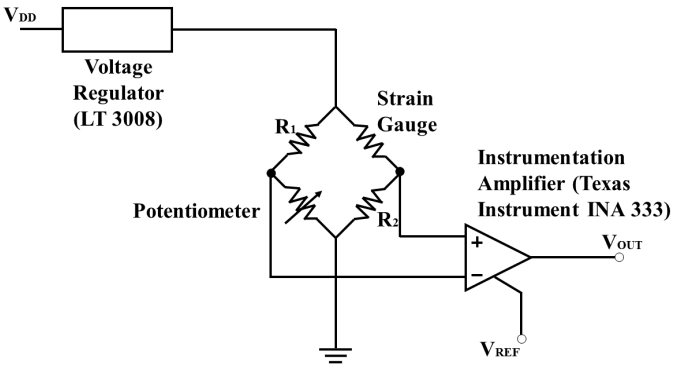

Fig. 5. Wheatstone bridge circuit diagram.

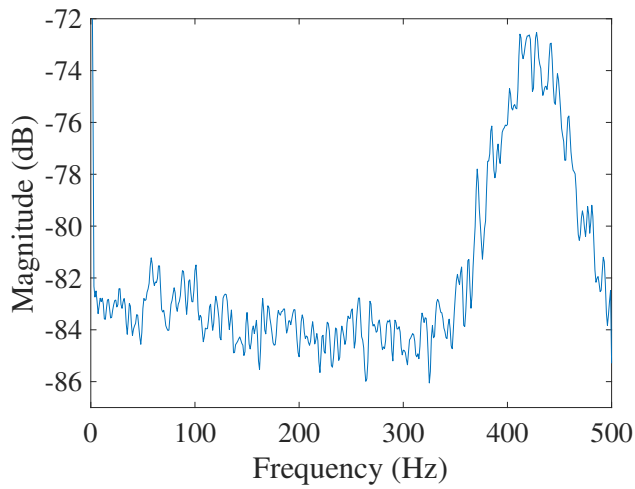

Fig. 6. Power spectral density estimate for quiescent noise.

F. Encapsulation

Gauge and electrical trace elements are covered with a final 10 μm thick layer of Parylene C as a hermetic seal in order to minimize oxidation (which could negatively affect gauge performance). An additional benefit of this layer is to serve as a barrier for sterilization for medical devices. The layer is manufactured using a chemical vapor deposition (CVD) technique and a pre-patterned Kapton tape mask is aligned to the tool before the polymer deposition. The electrical connections to the gauges are wired before the encapsulation process.

G. Electronics

Changes in resistance are measured with a basic Wheatstone bridge used in quarter-bridge configuration as shown in Fig. 5. Despite printing two sensors and having the opportunity to use the circuit as a half-bridge configuration to further amplify the signal, the simplest setting was chosen to improve consistency of the circuit and eliminate the need to match resistance between two strain gauges. The board includes a magnet mounted 3.7 V Li-Po battery as its power source, an LT 3008 adjustable voltage regulator (Linear Technology) set to an output of 2.0 V, an INA333 differential operational amplifier (Texas Instruments) and a tunable potentiometer. The adjustable instrumentation differential amplifier has its gain set to 500 to improve overall signal output. System noise measured at the amplifier input is 0.0186 V/$\sqrt{\text{Hz}}$.

All tests conducted use the quarter bridge configuration to characterize the sensitivity of a single gauge. However, a half-bridge configuration could be implemented by replacing R_2 in Fig. 5 with a strain gauge that is parallel to the original strain gauge on opposite side of the shaft. Adding this gauge would improve the signal to noise ratio because the voltage changes for each input of the instrumentation amplifier would be larger.

To analyze the frequency composition of the output noise, we connect a strain gauge to the circuit and record the output voltage without applying any strain. Fig. 6 shows the power spectral density for this quiescent data. At low frequencies, the noise is quite low; the magnitude makes sense considering the noise produced by resistors, the strain gauge, and other electronic components.There is a considerable amount of noise around 400 Hz. The cause of this noise is a 400 Hz power supply located in the same room tests were conducted. This demonstrates that the gauge is susceptible to electromagnetic interference.

H. EMI Shielding

Surgical rooms are populated with multiple instruments that can create electromagnetic and electrostatic interference if not dealt with correctly. In order to improve the signal quality of the strain gauge sensor, an electromagnetic shielding will be included on both the top and the underside of the printed strain gauges and will be separated by an insulator layer. The shield will create a conductive enclosure (Faraday cage) which will reduce the susceptibility of the signal to electromagnetic fields, therefore improving the signal-to-noise ratio. As a basic concept test, a Faraday-type grid arrangement is deposited on the outer surface of the gauge and separated from it with an insulation layer. Here, the enclosure is optimized to suppress frequencies of up to 5.8 GHz as described by the IMS band (Industrial, Scientific and Medical band) of the electromagnetic spectrum. Electrosurgery and electrocautery require high frequencies, for example the typical frequency used for electrosurgery is around 0.5 MHz, to ensure that the current goes through the patient's tissue without producing electrical shocks to the skin [22].

This shield is incorporated in the manufacturing process of the strain gauges as explained in Section II. After encapsulating the strain gauge, the sample is inserted back inside the sputter coater to deposit a metallic layer (copper) that forms the outer shielding. The shield design is manufactured using two different masks to integrate the required features. First, rectangular conductive pads are printed perpendicularly to the gauge, as shown in Fig. 7. Once this first coating is deposited, an additional mask is placed perpendicular to this last one to form the grid. The conductive grid was applied on top of each strain gauge and a printed copper

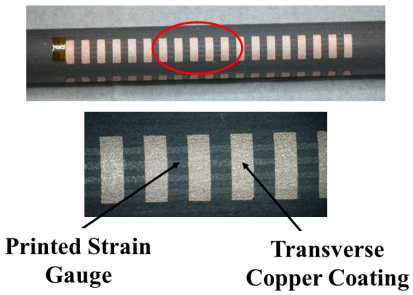

Fig. 7. Fiberglass shaft and detail of the transverse coating that forms the shield.

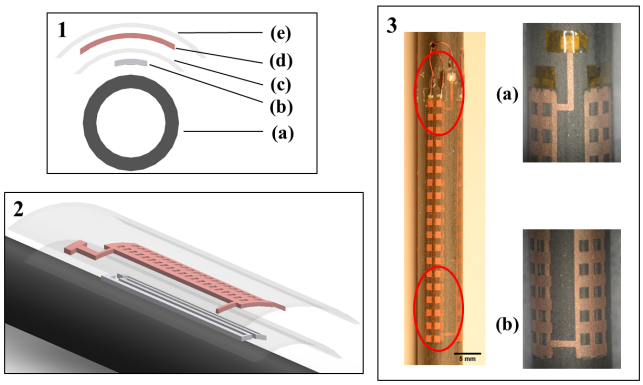

Fig. 8. **(1)** Schematic cross section of the fiberglass shaft and layer-up after printing the sensor and the EMI shield: (a) Substrate: Composite shaft that does not need to be insulated due to its non-conductivity. (b) Metallization: Carried out in the sputter coater. The materials used are Constantan or Karma, and the total thickness of the sensor is approximately 1 μm. (c) Encapsulation: Layer of Parylene C (approximately 10 μm) that encapsulates the sensor and avoids contact between the gauge and the shielding. (d) Metallization: Copper shield with approximately 1 μm thickness. (e) Encapsulation: Layer of Parylene C (approximately 10 μm) that encapsulates the metallization and prevents degradation. **(2)** Schematic exploded view of the layer-up. The layer-up consists of four layers, metallization (gauge and shield), and insulation and encapsulation layers. **(3)** Intuitive Surgical composite shaft and encapsulated EMI shielding made of copper (underneath there is the strain gauge): (a) Trace used to ground the shield. (b) Detail of one of the traces that connects two grids to ensure proper grounded.

trace connects the shielding of each strain gauge element to guarantee proper grounding of the Faraday cage. In the final version, printed electrical traces from the strain gauges will run beneath the printed grounding traces to the Faraday shielding. This will provide an opportunity to capacitively bypass the gauge signal leads to the Faraday shield as they exit the shield area.

The copper is deposited more rapidly than other materials, such as Constantan, at a rate of about 109 nm/min. After metallization, the mask is removed and the sample is returned to the parylene coater for a final encapsulation of a thin layer of biocompatible polymer material (Parylene C) to prevent damage. A detailed image is shown in Fig. 8.

An EMI shielding concept test is performed in an anechoic chamber which absorbs reflections of electromagnetic waves and is also insulated from exterior sources of noise. As it is

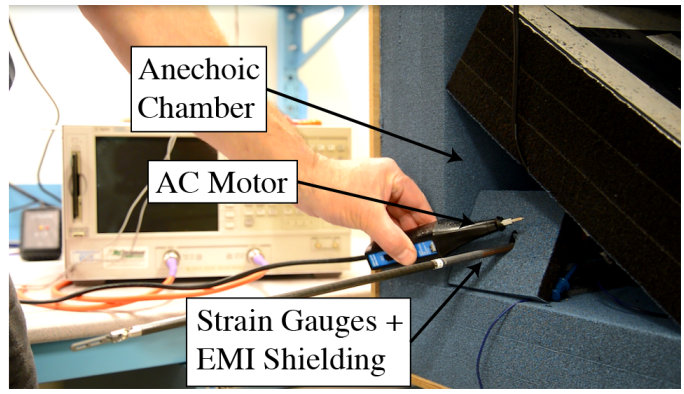

Fig. 9. EMI shielding testing configuration.

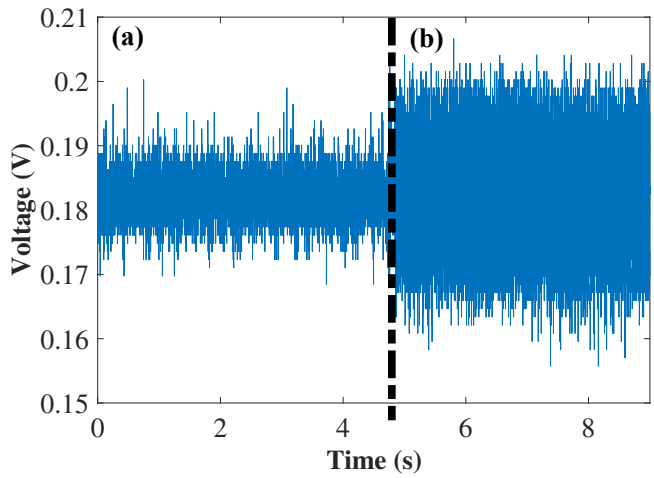

Fig. 10. Robustness to EMI interference with and without EMI shield grounding: (a) Interference from external source is introduced with EMI shield grounded. (b) Interference from external source is introduced with EMI shield not grounded, resulting in observable signal amplitude change.

shown in Fig. 9, the proximal end of the end effector and the electronics are placed inside the chamber, leaving the strain gauge and shielding outside to be tested. The goal of this exercise is to conduct a preliminary test of the outer shield by monitoring the signal output, while an AC motor is switched on close to the end effector as a representative noise source (this test noise source is substantially lower in frequency and intensity than a cautery noise source would be). The signal, when the shield is grounded and the AC motor disturbs the environment, results in peak to peak voltage amplitude of approximately 30 mV, shown in Fig. 10, part (a). Furthermore, if the shield is disconnected, the signal output increases to 50 mV, as shown in Fig. 10, part (b) indicating the partial shielding has some effect on the induced EMI.

IV. Testing and Results

Gauge characterization is conducted on an Instron 5544 materials tester with a Versa-Channel peripheral transducer for voltage input during surface strain testing. Signal processing during Inston testing is provided by an in-house manufactured circuit board with analog electronics as described

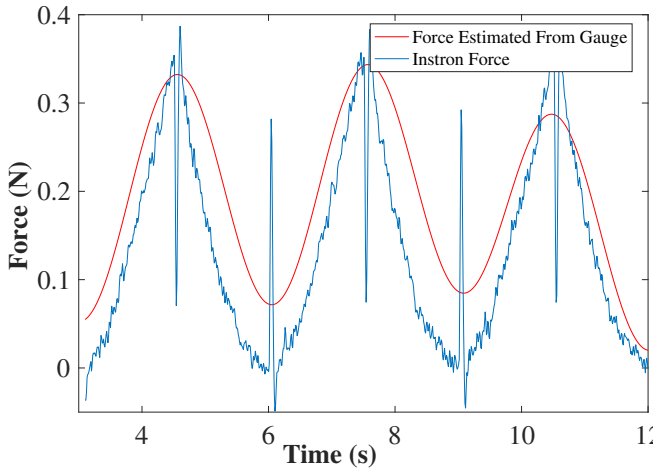

Fig. 11. Instron 2.5mm Needle Driver sensitivity test.

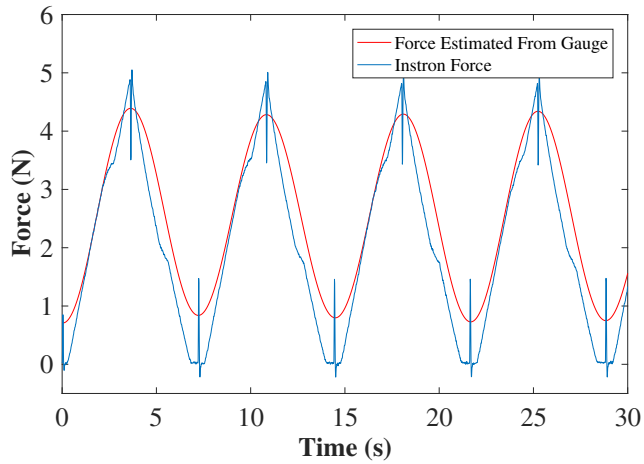

Fig. 12. Instron 30mm Needle Driver cyclic test.

in Section III, subsection G. In an effort to recreate the clamping and deflection experienced during actual usage, the Intuitive Surgical Fenestrated Grasper and the Needle Driver proximal ends are clamped at testing height horizontally and supported by an adjustable lab jack. Downward force on the distal end is exerted by the Instron, straining the sensorized surface. The composite shaft of the end effector is moved at 100 mm/sec and force is detected with a 2 KN Instron load cell. Sensitivity is evaluated during cyclic deflection tests of 2.5 mm which require forces of 400 mN (Fig. 11) shown in blue. Force spikes are seen at the peaks and the valleys of the Instron data due to the inertial effects on the load cell resulting from reversing the cross head. During the deflection tests, data received from the printed strain sensor (shown in red) is digitally filtered using a Butterworth 1st order filter set to a 10 Hz cutoff (3 dB). The comparison of the precise Instron force data is in close correlation to the printed sensor data in phase ($0.71°$), slope (within $2.1°$) and amplitude (amplification dependent).

The lower limit of strain sensing resolution is defined by the test system noise floor which is 15.9 mV, primarily due to induced noise from the Instron lead screw motor. This proves to be a good baseline for actual operating conditions as equipment in the surgical suite is expected to create substantial background EMI which is addressed in Section III, subsection H. Instron cyclic testing at a deflection of 30 mm requires forces of 5 N (well above typical tissue pretension needs) and is shown in Fig. 12. Similar to the sensitivity testing, precise force data is compared with gauge output which is filtered using a Butterworth 1st order low pass filter set to a 10 Hz cutoff (3 dB). Analysis of the Instron force data (Fig. 12, shown in blue) reveal substantial inertial effects exerted on the load cell from the motion of the cross-head due to the high feed rate. This shows up as a substantial decrease in force (at the peak) and a substantial increase in force (at the valley) of each test cycle. Evidence of slippage between the cross-head load cell contact point and the composite shaft is also evident at the 3.4 N point on the downward movement (shown as positive force) during the four cycles shown in this test. This is a result of contact point movement as the shaft deflects. As positive force is exerted on the shaft there is close correlation between the precise Instron force data and the printed strain gauge data in phase (0.84 degrees delay of the gauge signal), slope (0.04 degree deviation) and amplitude (amplification dependent). This deviation is repeated through the four cycles shown in the figure. A comparison of the negative slope side of each of the four cycles show some slope deviation in the response of the gauge in comparison to the response of the Instron load cell. Here the force estimated from the gauge varies in slope from the precise Instron force by 4.6 degrees. This is a result of the composite shaft slipping relative to the Instron load cell contact point as the shaft straightens.

During limit testing of extreme fiber strain on the Fenestrated Grasper shaft (3000 $\mu\epsilon$ at the gauge location), a single distal end deflection of 43 mm requires a force of 12 N and results in an output voltage of 410 mV peak to peak. Precision and repeatability are examined by analysis of digitally filtered gauge data using a Butterworth 1st order low pass filter at 10 Hz. In order to verify the sensor response, an extension cyclic test was performed in which the Instron machine was set to apply 1200 extension cycles of up to 30 mm at the tip of the instrument. Fig. 13 shows the sensor response, as it can be seen, during the first 100 cycles of the test, the sensor response shows a clear variation in voltage relative to the extension of the instrument. When comparing the first 100 cycles to the last 100 cycles of the test it can be seen that there is a drift of the measurement of $\sim$0.02V. Future work will focus on identifying causes of this drift to prevent it, moreover, for multiple applications in which the position of the instrument is known at some points of the procedure it may be possible to implement algorithms that reset this drift when the instrument is not supporting loads.

V. Conclusions and Future Research

We present an implementation of a novel method for printing low cost and low profile strain gauges on da Vinci robotic end effectors from Intuitive Surgical with the intent of providing tactile force feedback ability for the surgical

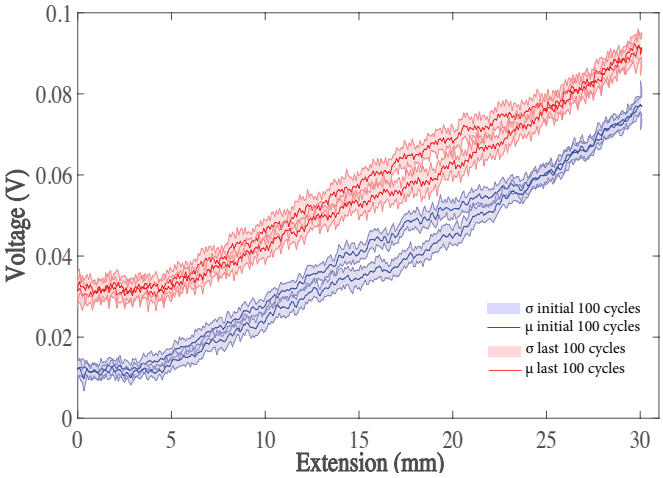

Fig. 13. Gauge repeatability and drift test by applying 1200 extension cycles. Blue line shows sensor response during the first 100 cycles and red line shows the sensor response during the last 100 cycles.

system. The low profile nature of the application fits well into the needs of the instrument operational space constraints (entry into the trocar, etc.) These sensors are placed onto the shafts with little or no surface preparation and minimal process steps. Gauges and electrical traces are hermetically sealed in a coating of Parylene C, making them compatible with accepted medical device encapsulation. Using printed sensors, the detectable forces perpendicular to the end-effector shaft range from 100 mN up to 12 N (in the extreme case). After an initial investment in processing equipment (up to $75,000), the materials to produce 1000 printed strain gauges cost ∼$0.09 per sensor. These costs do not include labor or maintenance costs. Although the current process includes manual steps (alignment jigs have been introduced to standardize the process), in this particular case, the strain gauges could be printed on the fiberglass shaft, before the final assembly. Also, numerous gauge trace configurations, orientations, and layer stackings are compatible with this technique and integrated signal processing is possible using the existing interface area with additional signal electronics inside the robot. In the future, our intention is to continue refinement of the gauge printing process and push signal detection and processing in order to improve the signal to noise ratio. We will implement a small scale deployment of printed sensors onto the da Vinci or similar robots to provide real time haptic feedback and to receive usage feedback from physicians in the field.

Acknowledgment

This work was supported by the Wyss Institute for Biologically Inspired Engineering and Intuitive Surgical Inc. (grant #A24708), which also contributed advice and feedback on the prototypes developed in this work. The prototypes were enabled by equipment supported by the ARO DURIP program (award #W911NF-13-1-0311).

References

[1] U. Kim, D. H. Lee, H. Moon, J. C. Koo, H. R. Choi, *Design and realization of grasper-integrated force sensor for minimally invasive robotic surgery,* Proc. IEEE/RSJ Int. Conf. Intell. Robot. Syst., pp. 4321-4326, Sep. 2014.

[2] A. R. Lanfranco, A. E. Castellanos, J. P. Desai, W. C. Meyers, *Robotic surgery,* Annal. Surgery, vol. 239, pp. 14-21, 2004.

[3] J. C. Hu, X. Gu, S. R. Lipsitz, M. J. Barry, A. V. D'Amico, A. C. Weinberg, N. L. Keating, *Comparative effectiveness of minimally invasive vs. open radical prostatectomy,* J. Amer. Med. Ass., vol. 302, no. 14, pp. 1557-1564, 2009.

[4] E. J. Hanly, M. A. Talamini, "Robotic abdominal surgery, *Amer. J. Surgery,* vol. 188, pp. 19S-26S, 2004.

[5] U. Kim, D. H. Lee, W. J. Yoon, B. Hannaford, H. R. Choi, *Force Sensor Integrated Surgical Forceps for Minimally Invasive Robotic Surgery,* IEEE Transactions on Robotics, Vol. 31, issue 5, Oct. 2015.

[6] J. C. Chiao, J. M. Goldman, D. A.Heck, P. Kazanzides, W. J. Peine, J. B. Stiehl, D. Yen, N. G. Dagalakis, *Metrology and Standards Needs for Some Categories of Medical Devices,* Journal of Research of the National Institute of Standards and Technology. pp.121-129, 2008.

[7] T. Ranzani, G. Ciuti, G. Tortora, A. Arezzo, S. Arolfo, M. Morino, A. Menciassi, *A Novel Device for Measuring Forces in Endoluminal Procedures,* International Journal of Advanced Robotic Systems, 2015.

[8] S. McKinley, A. Garg, S. Sen, R. Kapadia, A. Murali, K. Nichols, S. Lim, S. Patin, P. Abbeel, A. M. Okamura, K. Golberg, *A Single-Use Palpation Probe for Locating Subcutaneous Blood Vessels in Robot-Assisted Minimally Invasive Surgery,* IEEE International Conference on Automation Science and Engineering (CASE), Aug. 2015.

[9] J. Back, P. Dasgupta, L. Seneviratne, K. Althoefer, H. Liu, *Feasibility Study-Novel Optical Soft Tactile Array Sensing for Minimally Invasive Surgery,* IEEE/RSJ International Conference on Intelligent Robots and Systems (IROS), Germany, Sep. 2015.

[10] C. J. Payne, H. Rafili-Tari, H. J. Marcus, G. Z. Yang, *Hand-Held Microsurgical Forceps with Force-Feedback for Micromanipulation,* IEEE International Conference on Robotics and Automation (ICRA), Jun. 2014.

[11] K. Rebello, *Applications of MEMS in Surgery,* Proceedings of the IEEE, vol. 92 no. 1, pp. 43-55, 2004.

[12] Z. Sun, M. Balicki, J. Kang, J. Handa, R. Taylor, I. Iordachita, *Development and preliminary data of novel integrated optical micro-force sensing tools for retinal microsurgery,* IEEE Int. Conf. Robot. Autom., pp. 1897-1902, 2009.

[13] F. Hammond, R. Kramer, Q. Wan, R. Howe, and R. Wood, *Soft Tactile Sensors for Micromanipulation,* IEEE Int. Conf. on Intelligent Robotics and Systems, Vilamoura, Portugal, pp. 25-32, Sep. 2012.

[14] P. Saccomandi, E. Schena, C. M. Oddo, L. Zollo, S. Silvestri, E. Guglielmelli, *Microfabricated Tactile Sensors for Biomedical Applications: A Review,* Biosensors, vol. 4 no. 4, pp. 422-448, 2014.

[15] S. Sokhanvar, M. Packirisamy, J. Dargahi, *A Multifunctional PVDF-based tactile sensor for Minimally Invasive Surgery,* Smart Materials and Structures, 16(4), pp.989-998.10.1088/0964-1726/16/4/006, 2007.

[16] Y-L. Park, S. Elayaperumal, S. Ryu, B. Daniel, R. J. Black, B. Moslehi, M. R. Cutkosky, *MRI-compatible Haptics: Strain sensing for real-time estimation of three-dimensional needle deflection in MRI environments,* Int. Society for Magnetic Resonance in Medicine, 17th Scientific Meeting, and Exhibition, Honolulu, Hawaii, 2009.

[17] Y-L. Park, S. Elayaperumal, B. Daniel, S. C. Ryu, M. Shin, J. Savall, R. J. Black, B. Moslehi, M. R. Cutkosky, *Real-Time Estimation of 3-D Needle Shape and Deflection for MRI-Guided Interventions,* IEEE ASME Transactions on Mechatronics, Vol. 15, Issue 6, Dec. 2010.

[18] B. Zhao, C. A. Nelson, *Estimating Tool-Tissue Forces Using a 3-Degree-of-Freedom Robotic Surgical tool,* ASME Journal Mechanical Robot, Oct. 2016.

[19] F. L. Hammond, M. J. Smith, R. J. Wood, *Estimating Surgical Needle Deflection with Printed Strain Gauges,* 36th Annual International Conference of the IEEE Engineering in Medicine and Biology Society, Chicago, IL, pp.6931-6936, 2014.

[20] R.L. Hannah, *Strain Gage Users' Handbook*. New York: Springer. p. 50. ISBN 978-0412537202, 1992.

[21] *Properties of Some Metals and Alloys*. The International Nickel Company, Inc. 1982

[22] Bovie Medical Corporation, *http://blog.boviemed.com/blog-1/3-key-differences-between-electrosurgery-electrocautery*